Analysis of Intermediates and Products from the Dehydrogenation of $Mg(BH_4)_2$

Iffat H. Nayyar[1], Bojana Ginovska[1], Mark Bowden*[1], Gary Edvenson[2], Ba Tran[1] and Tom Autrey[1]*

[1]Physical Sciences Division, Physical and Computational Sciences Directorate, Pacific Northwest National Laboratory, Richland, WA 99354, USA

[2]Chemistry & Biochemistry Department, Minnesota State University, Moorhead, MN 56563 USA

*Corresponding authors: bojana.ginovska@pnnl.gov; mark.bowden@pnnl.gov

Abstract. The thermodynamic properties of key compounds, $Mg(B_3H_8)_2$, MgB_2H_6, $MgB_{10}H_{10}$, $Mg(B_{11}H_{14})_2$, $Mg_3(B_3H_6)_2$, and $MgB_{12}H_{12}$, proposed to be formed in the release of hydrogen from magnesium borohydride $Mg(BH_4)_2$ and uptake of hydrogen by MgB_2, have been investigated using solid–state density functional theory (DFT) calculations. More accurate treatment of cell–size effects to the entropies were also investigated, in order to improve the accuracy of the thermodynamic properties of complex borohydrides. We find that the zero–point energy corrections can lower the electronic energies of reaction by 20–30 kJ/(mol H_2) for these intermediates, while adding the thermal and entropy contibutions results in the total decrease up

to ~50 kJ/(mol H_2). Although our treatment lowers the calculated formation energy of $Mg(B_3H_8)_2$, it is still too high to explain the experimental observation of $B_3H_8^-$. We discuss possible reasons for this disparity and propose that the formation of $B_3H_8^-$ and H^- in a disordered amorphous phase has a large energy difference compared to the phase–separated $Mg(B_3H_8)_2$ and MgH_2 considered in calculations. Comparison of the experimental and NMR chemical shifts calculated within a DFT approach for known species $Mg(BH_4)_2$, $Mg(B_3H_8)_2$, $Mg(B_{11}H_{14})_2$, $MgB_{10}H_{10}$ and $MgB_{12}H_{12}$ provides validation for predicting the chemical shifts of the other compounds which are yet to be confirmed experimentally. These include MgB_2H_6 and the proposed tri–anion species $Mg_3(B_3H_6)_2$ that both have favorable thermodynamics for reversible hydrogen storage in $Mg(BH_4)_2$ without the formation of MgH_2 as a co–product which could phase–separate and inhibit rehydrogenation.

1. Introduction

With the increasing availability of excess electricity from renewable resources on a grid scale there is a critical need to develop technologies capable of storing and transporting energy on a large scale.[1] Electrolysis to make green hydrogen and storing it in chemical bonds is an approach to provide geographically agnostic energy storage that spans a range of capacity and time scales.[2-3] Compounds that readily release H_2 when initiated by a change in temperature and/or pressure have the potential to enable a wide variety of applications including energy storage for a microgrid neighborhood, i.e., 30 kW for 6 months (ca. 90 MWh), to emergency backup power for data centers, i.e., > 20 MW for 3 days (ca. 1500 MWh).[3]

Hydrogen rich materials such as magnesium borohydride, $Mg(BH_4)_2$ are candidates of interest owing to the abundance of magnesium and boron, a high hydrogen density, ca. 149 g H_2/kg, and a low thermodynamically predicted dehydrogenation temperature (75 °C) to form MgB_2.[4] However, in practice large kinetic barriers result in high temperatures for release and high pressures for regeneration. For example, dehydrogenation temperatures > 450 °C are required to form MgB_2,[5] and pressures greater than 900 bar are needed to reform $Mg(BH_4)_2$.[6] On the other hand, H_2 is released at temperatures < 200 °C to form *partially* dehydrogenated hydridoborate intermediates, e.g., $Mg(B_3H_8)_2$, which can be rehydrogenated under moderate pressure to reform $Mg(BH_4)_2$.[7-8] This has sparked interest from the research community to identify intermediate products deeper in

the dehydrogenation cycle which provide more hydrogen[9-11] and can be regenerated under moderate temperature and pressure.

The efficient release and subsequent regeneration of a hydrogen storage material can be best realized when the free energy change for the reaction is close to zero. Assuming the entropy loss for uptake of H_2 to reform borohydride from a range of intermediate products is ca. 100 ± 15 J/(K mol H_2)[4] limits the enthalpy of H_2 release to a relatively narrow window of ca. 30–40 kJ/(mol H_2). If the enthalpy (ΔH) is $<$ 30 kJ/(mol H_2), H_2 release will be favorable, however high pressures of H_2 will be required to regenerate the borohydride. On the other hand, if the enthalpy is > 40 kJ/(mol H_2), regeneration will be favorable but high temperatures will be required to release hydrogen.

This thermodynamic view does not clarify experimental observations of $Mg(B_3H_8)_2$ as a major dehydrogenation product of $Mg(BH_4)_2$ at lower temperatures.[7] Specifically, the observation of a reversible pathway connecting $Mg(BH_4)_2$ and $Mg(B_3H_8)_2$ at temperatures < 250 °C is contrary to a computational study[12] that suggests that the $Mg(B_3H_8)_2$ intermediate is highly unstable, ΔH ca. 150 kJ/(mol H_2), and should not be formed at temperatures below 1000 °C. Further, the same study calculates that dehydrogenation to $Mg_3(B_3H_6)_2$ does lie within the optimum thermodynamic window, ΔH = 40 kJ/(mol H_2), yet this compound has not been observed as an intermediate, raising a number of questions: What pathways would lead to formation of this unique trianion? Is $B_3H_8^-$ a precursor to $B_3H_6^{3-}$ or vice versa – or do the two triborate species arise from different pathways?

Plane wave density functional theory (DFT) calculations are commonly used to predict reaction enthalpies with the goal of identifying promising reactions having the capability to exhibit reversible hydrogen storage in hydridoborate materials at moderate temperatures and pressures.[13-15] The emphasis in the current work is on the inclusion of vibrational and thermal contributions to the electronic energies, while employing larger cell sizes to examine the effect on the predicted thermochemistry of the reactions. We discuss reasons for the experimental observation of $Mg(B_3H_8)_2$, and investigate the thermodynamic properties of other possible intermediates on the reaction pathway from $Mg(BH_4)_2$ to MgB_2. These provide additional compounds that researchers can target for new storage systems. DFT calculations of ^{11}B NMR chemical shifts are benchmarked against known hydridoborate species, and are used to predict the NMR signature of intermediates that have no experimental spectra.

2. Computational Methods

Thermodynamic and NMR calculations for the solid–state periodic systems were performed within the DFT approach using the Vienna *ab–initio* simulation package (VASP) code[16] and the ultrasoft pseudopotentials and PBE[17-18] functional within the projector augmented wave (PAW)[19] scheme. All atomic positions and cell parameters were relaxed until the forces and stress on each of the unconstrained atoms were below 0.01 eV/Å and 0.2 kbar, respectively. The plane–wave basis with an 875 eV cutoff and a choice of 36 *k*–points Monkhorst–Pack grid has yielded energies converged up to 10^{-10} eV/*f.u*. Finite temeperature effects were added using the phonon density of states calculated within the density functional perturbation theory using VASP and Phonopy[20] codes. The NMR chemical shift (δ) for all the atoms of the borohydride intermediates were calculated from their absolute chemical shielding (σ) values obtained from DFT, using boron trifluoride etherate ($BF_3 \bullet Et_2O$) as a refrence. The structures and NMR shifts for small molecule models were also calculated within the DFT approach using the NWChem program.[21] Molecular diagrams were prepared using Vesta[22] and details of the computational approaches used and calculation methods are provided in the sections S1, S2 and S3 of the SI.

3. Results and Discussion

3.1 Thermodynamic stability and boron NMR chemical shifts for $Mg(BH_4)_2$ polymorphs

$Mg(BH_4)_2$ is observed in several polymorphs at room temperature. The first described were α–$Mg(BH_4)_2$ (space group $P6_122$)[23] and an orthorhombic structure[24] denoted as β–$Mg(BH_4)_2$ which is formed after an endothermic phase transition above ca. 200 °C. The transition is not reversible and β–$Mg(BH_4)_2$ persists if the specimen is cooled. More recently a cubic γ polymorph[25] has been reported which has an open framework structure able to absorb molecular H_2 under high pressure at low temperature. Although not observed experimentally, an additional tetragonal structure[26] was predicted using the *PEGS* Monte Carlo method for structure prediction.[27] Since β–$Mg(BH_4)_2$ is metastable at room temperature, we have carried out DFT calculations on the α, γ, and *PEGS* polymorphs to compare their stability and calculate their NMR chemical shifts.

Table 1. Calculated energies ΔE, enthalpies ΔH, and solid–state ^{11}B NMR chemical shifts δ (relative to $BF_3 \bullet Et_2O$) for different polymorphs of $Mg(BH_4)_2$. The energies and enthalpies are calculated for the reaction $MgB_2 + 4H_2 \rightarrow Mg(BH_4)_2$ at 0 and 300 K, respectively.

Polymorph	ΔE	ΔH	^{11}B δ **(ppm)**	
	(kJ/mol)		**Calc.**	**Expt.**
γ-$Mg(BH_4)_2$	-210.4	-146.1	-41.2	-41[28]
PEGS	-205.9	-139.1	-42.2	–
α-$Mg(BH_4)_2$	-201.3	–	-38.7, -40.2 *(4:1)*	-39.3, -40.8 *(4:1)*[5]

Several theoretical studies[26, 29-31] have examined polymorphism in $Mg(BH_4)_2$ and proposed a range of possible structures with similar formation energies. These studies have noted the complexity of α–$Mg(BH_4)_2$ which has 330 atoms, i.e. 30 $Mg(BH_4)_2$ formula units, in the unit cell which makes accurate calculations computationally demanding. The β–$Mg(BH_4)_2$ polymorph, is even more complex, with 704 atoms, and since previous calculations showed that the enthalpy of transition from α to β is 9-14 kJ/mol,[27-29] it is less stable than α–$Mg(BH_4)_2$ and was not considered in this work. By comparison, γ–$Mg(BH_4)_2$ has 12 formula units and the *PEGS* structure only 4 formula units in their respective unit cells. We calculated the electronic energy and the enthalpy (Table 1) for the formation of $Mg(BH_4)_2$ from MgB_2 according to equation (1):

$$MgB_2 + 4H_2 \rightarrow Mg(BH_4)_2. \quad (1)$$

The large number of atoms in the α–$Mg(BH_4)_2$ unit cell makes calculation of the vibrational and thermal corrections prohibitively expensive, and calculation of ΔH for this polymorph was omitted. Compared to the *PEGS* structure, we find ΔE for the γ polymorph to be 4.5 kJ/mol lower in energy and α–$Mg(BH_4)_2$ 4.6 kJ/mol higher. The enthalpy at 300 K for the *PEGS* polymorph is lower in energy by 7 kJ/mol than for γ–$Mg(BH_4)_2$. The minor differences in both energy and enthalpy are well within the accuracy of the methods. Our calculations are not intended to accurately predict the stability of observed or proposed polymorphs, but to establish a baseline for subsequent calculations of dehydrogenation energies. Consequently, calculations for the energies of

dehydrogenation presented later in the current work are referenced to the *PEGS* polymorph in order to provide direct comparison with the previous published[12] values.

The calculated ^{11}B NMR chemical shifts (δ_{calc}) for the $Mg(BH_4)_2$ polymorphs (Table 1) show very good agreement with experimentally reported (δ_{expt}) values. The computed shifts for the γ polymorph (-41.2 ppm) and the *PEGS* structure (-42.2 ppm) are within 1 ppm of the experimental γ–$Mg(BH_4)_2$ value. For the α polymorph, the calculated chemical shifts cluster into two groups with averages of -38.7 and -40.2 ppm and numbers of Mg atoms in the ratio 4:1. The presence of these nonequivalent boron sites explains the ^{11}B MAS–NMR spectrum reported by Soloveichik *et al*.[5] who found similar chemical shifts in the same intensity ratio (Table 1). There is little variation in the chemical shifts for all the polymorphs as they contain very similar local configurations: Mg atoms surrounded by four BH_4^- groups in a tetrahedral configuration which in turn coordinate to a further Mg atom through opposite edges.

3.2 Boron NMR chemical shifts for $Mg(BH_4)_2$ dehydrogenation intermediates

Table 2. Calculated solid–state ^{11}B NMR chemical shifts δ relative to $BF_3 \cdot Et_2O$ compared with available measurements. Entries marked with * are for the K salt of the relevant anion in solution.

Compound	**^{11}B δ_{calc} (ppm) Solid–state**	**^{11}B δ_{expt} (ppm)**	
		Solid–state	**Solution**
$Mg(B_3H_8)_2$	-30.6	-27.0, -31.6, -34.0[32]	-30.3[8]
$Mg(B_{11}H_{14})_2$	-12.5, -15.6, -16.7 *(1:5:5)*	–	-12.5, -14.1, -14.9 *(1:5:5)**[33]
MgB_2H_6	-44.8	–	-27*[34]
$MgB_{10}H_{10}$	+3.6, -23.8 *(1:4)*	-2, -27 *(1:4)*[11]	-1, -30 *(1:4)*[8]
$Mg_3(B_3H_6)_2$	-47.2	–	
$MgB_{12}H_{12}$	-13	-12[5, 35]	-15[8]

The calculated NMR ^{11}B chemical shifts for intermediates in the dehydrogenation of $Mg(BH_4)_2$ are reported in Table 2 and compared with experimentally measured values where known. The structures of the anions are reported in Figure 1.

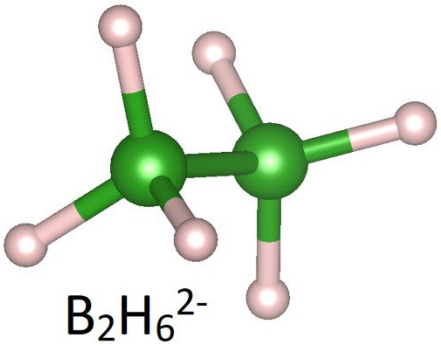

$B_2H_6^{2-}$

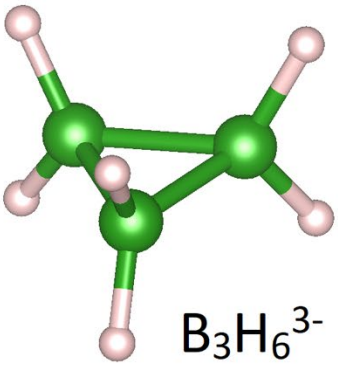

$B_3H_6^{3-}$

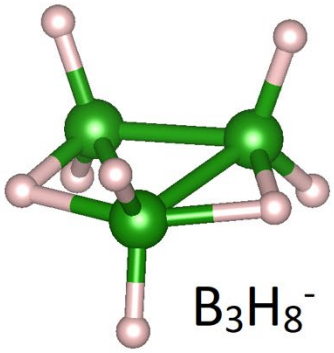

$B_3H_8^-$

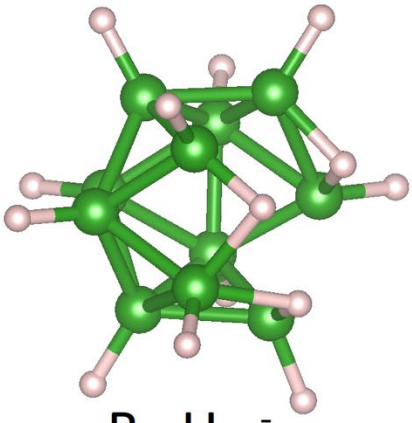

$B_{11}H_{14}^-$

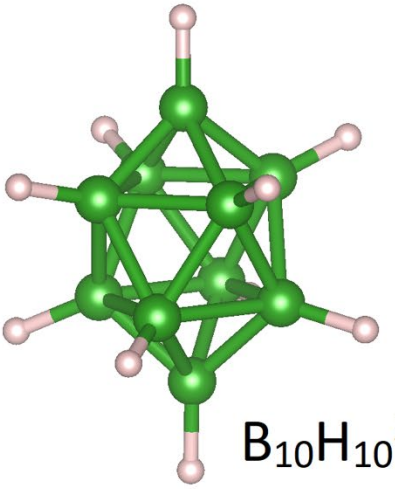

$B_{10}H_{10}^{2-}$

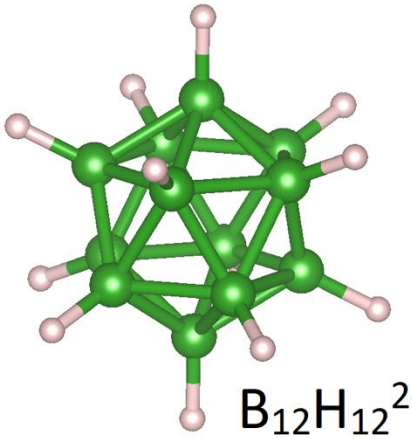

$B_{12}H_{12}^{2-}$

Figure 1: Molecular structures of the anions of the magnesium hydridoborates considered as intermediates or products in this study. Boron atoms are depicted as green spheres and hydrogen atoms as white spheres.

There are relatively few reported solid–state spectra where the identities of species have been independently confirmed. However, chemical shifts from solution NMR experiments are more widely available and are often close to their solid–state counterparts. The predictions in Table 2 show excellent agreement with experiment and provide confidence for interpretation of new resonances observed in *in–situ* NMR spectroscopic measurements. We observe that the calculated chemical shift for $Mg(B_3H_8)_2$ is in exact agreement with the experimental peak observed by solution NMR, and falls well within the range observed in solid–state experiments.[32] For $Mg(B_{11}H_{14})_2$, $MgB_{10}H_{10}$, and $MgB_{12}H_{12}$ the calculations show very good agreement with experimental measurements, both for the chemical shifts and the ratio of the site populations.

The NMR shifts for MgB_2H_6 and $Mg_3(B_3H_6)_2$ crystals are predicted to be at -44.8 and -47.2 ppm respectively, but to date no solid–state NMR data have been reported for these compounds. For MgB_2H_6, the calculated NMR chemical shift differs considerably from its experimentally measured solution value (-27 ppm, for $K_2MgB_2H_6$ and $Rb_2B_2H_6$ solutions[34]). To investigate this further, we calculated chemical shifts for molecular MgB_2H_6 clusters in the gas phase that are likely to be closer to the environments found in solution, where rotation about the B-B bond is more available due to the lack of lattice constrains, giving rise to richer conformational space. We found a range of chemical shifts, varying from -8 to -45 ppm, which were sensitive to the geometry of the available conformers found to be stable in gas phase (see Figure S1). The calculations included a single MgB_2H_6 cluster, as well as $Mg(B_2H_6)_2$ ions where the position of Mg^{2+} differs for each of the $B_2H_6^{2-}$ anions. The average of the calculated chemical shifts for all of these conformers is ~ -27 ppm, in agreement with the reported solution shift[34] (see Table S1). Notably, the gas phase structure with a boron environment closest to the solid-state crystal structure has a chemical shift of -45 ppm, in excellent agreement with the solid -state calculation (Figure S2). For comparison, we also calculated the gas–phase NMR shifts for $K_2B_2H_6$, the system reported in the Shore *et al*.[34] In this case, since K^+ is a monovalent ion, there is even larger range of possibilities for various conformations. We calculated a number of those conformers (Figure S3) and reported their chemical shifts in Table S2. The average of the shifts from these structures is ~ -28 ppm, again in very close agreement with the reported experiental value.

For consistency, we also undertook the same gas phase calculations for $Mg(B_3H_8)_2$. We calculated 5 different isomers for this system, with the NMR shifts ranging form -27 ppm to -33 ppm. This narrower range demonstrates that for this compound, the sensitivity of the NMR resonance to the different conformations is much smaller. The overall average of these conformers is ca. -30 ppm, which is in excellent agreement with the solid state and solution state NMR measurements and the solid state calculated values reported in Table 2. The calculated isomers are reported in Figure S4 and the NMR shifts are provided in Table S3.

These calculations show that care must be taken when solution NMR chemical shifts are used to identify species from solid–state spectra. In the majority of cases the chemical shifts are close to one another, but for compounds like MgB_2H_6 the crystal packing can constrain the range of available boron geometries and give rise to different observed NMR resonances. This would not affect anions like BH_4^- or the larger and more rigid closo–boranes like $B_{10}H_{10}^{2-}$ and $B_{12}H_{12}^{2-}$, but can be a factor in smaller anions like $B_2H_6^{2-}$.

3.3 Thermodynamic stability for $Mg(BH_4)_2$ dehydrogenation intermediates

The calculated reaction enthalpies and free energies for possible intermediates from $Mg(BH_4)_2$ dehydrogenation can help address the question of the feasibility of different reaction pathways that can lead to formation of products with various stabilities. The calculated thermodynamic quantities for reactions forming $Mg(B_3H_8)_2$, $Mg(B_{11}H_{14})_2$, MgB_2H_6, $MgB_{10}H_{10}$, $Mg_3(B_3H_6)_2$, MgB_2 and $MgB_{12}H_{12}$ are given in Table 3 and compared with previously published[12] values where available.

Table 3**:** Calculated thermodynamic quantities for reaction pathways forming various metastable metal borohydride intermediates from the dehydrogenation of $Mg(BH_4)_2$. The formula units (*f.u.*) are specified for the borohydride intermediates formed during the dehydrogenation reaction of $Mg(BH_4)_2$. Here, ΔE is the electronic total energy without the zero point energy (zpe) corrections at 0K; ΔE_{zpe} and ΔH are the energies and enthalpies with vibrational corrections at 0 and 300 K, respectively; ΔS and ΔG are the entropy and Gibb's free energy at 300 K. Literature values are from Zhang et al.[12]

Dehydrogenation reaction intermediates MgB_xH_y	**Formula units of MgB_xH_y**	***ΔE***		***ΔE$_{zpe}$***		***ΔH***		***ΔS***		***ΔG***	**Mass Loss**
		0 K				**300 K**					
		kJ/(mol H_2)						**J/(K mol H_2)**		**kJ/(mol H_2)**	
			Lit.		**Lit.**		**Lit.**		**Lit.**		
$^1/_3$ $Mg(B_3H_8)_2$ + $^2/_3$ MgH_2 + $^2/_3$ H_2	1	176.3	180	148.7		147.9		65.5		128.2	2.5%
	4	176.3		148.7		149.7		84.9		124.2	
$^1/_{11}$ $Mg(B_{11}H_{14})_2$ + $^{10}/_{11}$ MgH_2 + $^{20}/_{11}$ H_2	1	77.5	81.1	53.3		55.4		89.8		28.5	6.8%
	2	77.5		53.3		55.4		89.9		28.5	
MgB_2H_6 + H_2	4	65.8	68.9	46.9	49.3	49.4	53.5	92.9	97.2	21.5	3.7%
$^1/_5$ $MgB_{10}H_{10}$ + $^4/_5$ MgH_2 + $^{11}/_5$ H_2	2	58.9	63	35.8		38.6		94.6		10.2	8.2%
	4	58.9		35.8		38.6		94.9		10.2	
$^1/_3$ $Mg_3(B_3H_6)_2$ + $2H_2$	4	53.6	57.4	35.3	34.7	37.9	40.2	94.3	108	9.7	7.5%
MgB_2 + 4 H_2	1	51.5	54.6	30.6	32.6	34.8	38.6	95.9	111.5	3.6	14.9%
$^1/_6$ $MgB_{12}H_{12}$ + $^5/_6$ MgH_2 + $^{13}/_6$ H_2	2	43.6	47.8	21	23.4	23.57	28.3	93.3	105.3	-4.4	8.1%

Our predicted electronic energies (ΔE) follow the similar trend computed by Zhang *et al.*[12] for the reactions, although our values are 3–4 kJ/(mol H_2) lower in energy. This difference is likely due to a small difference in the convergence criteria and is well within the acucarcy of the DFT. The zero point energy corrections (ΔE_{zpe}) applied within the harmonic approximation lower the energies by 20–30 kJ/(mol H_2). The calculated enthalpies are in the range 24 to 55 kJ/(mol H_2) for all the reactions except that to form $Mg(B_3H_8)_2$, which is 3–4 times higher at 149 kJ/(mol H_2).

The $Mg(B_3H_8)_2$ reaction also has a significantly smaller calculated entropy at 300 K (65.5 J/(K mol H_2)) compared to the other reactions, which fall in the range 90–96 J/(K mol H_2). This combination of large enthalpy accompanied by a smaller entropy change results in a large free energy (ΔG = 128 kJ/(mol H_2)) for the reaction to form $Mg(B_3H_8)_2$ at 300 K. The corresponding temperature in equilibrium with 1 atm H_2 gas, calculated simply by dividing ΔH by ΔS , is nearly 2000 °C, thus it is surprising that $Mg(B_3H_8)_2$ is one of the first observed species in the thermal dehydrogenation of $Mg(BH_4)_2$. The other reactions are considerably less endergonic, their free energies ranging from 29 to -4 kJ/(mol H_2). Consistent with experimental observations,[5, 35-36] the reaction forming $MgB_{12}H_{12}$ is the most thermodynamically favored amongst those investigated, with ΔG equal to -4 kJ/(mol H_2),.

The structures of the magnesium borohydride intermedates used for the calculations presented in Table 3 contain different numbers of formula units in their crystal unit cells depending on their symmetry constraints. For example, $Mg(B_3H_8)_2$ has just 1 formula unit per cell, while $Mg_3(B_3H_6)_2$ has 4. For products with fewer atoms in their unit cells, we also calculated the energy using larger super cell sizes, since the periodicity imposed by small cells can lead to larger errors associated with accurate calculation of the soft modes in the system. This did not change the calculated energies significantly except for the reaction entropy to form $Mg(B_3H_8)_2$, which increased from 65.5 to 84.9 J/(K mol H_2).

3.4 Reconciling the calculated instability of $Mg(B_3H_8)_2$ with experiment

Our use of vibrational corrections and larger cell sizes has lowered the 0 K calculated reaction enthalpy to form $Mg(B_3H_8)_2$ by ~30 kJ/(mol H_2). Taking account of the thermal and entropic contributions for the dehydrogenation to $Mg(B_3H_8)_2$ at typical reaction temperatures gives the

energies shown in Table 4. Although ΔS shows little dependence on temperature between 300 and 600 K, the TΔS term contributes significantly to the overall reaction energy, bringing the free energy of the reaction down to < 100 kJ/(mol H_2) at 600 K.

Table 4: Calculated enthalpy, Gibb's free energy, and entropy for reaction pathway leading to the formation of $Mg(B_3H_8)_2$ from $Mg(BH_4)_2$ in the temperature range 300 to 600 K.

T (K)	ΔH	ΔG	ΔS
	kJ/(mol H_2)		J/(K mol H_2)
300	149.7	124.2	84.9
400	149.8	115.7	85.2
500	150.1	107.1	85.9
600	150.4	98.5	86.5

However this is still highly unstable and leaves the question of why $Mg(B_3H_8)_2$ is the major product observed from dehydrogenation of $Mg(BH_4)_2$ at 473 K.[7] Further, why are the intermediates predicted to be stable like $MgB_{10}H_{10}$ and $MgB_{12}H_{12}$ not observed experimentally until higher temperatures, and appear to be formed *via* $Mg(B_3H_8)_2$?

We considered three explanations for the formation of $Mg(B_3H_8)_2$ despite its unfavorable calculated thermodynamics: *slow formation with a high barrier*, *entropic considerations* which have not been accounted for in computation, and *alternative solid–state forms* of $Mg(B_3H_8)_2$.

A. Kinetics of formation

The formation of $Mg(B_3H_8)_2$ as a product of $Mg(BH_4)_2$ decomposition was reported after a long time at a relatively low temperature;[7] approximately 25% conversion of BH_4^- to $B_3H_8^-$ was observed after heating under vacuum for 5 weeks at 473 K. An estimate of the activation barrier for this can be obtained from the Eyring equation:

$$k = \frac{k_B T}{h} e^{-\frac{\Delta G^{\ddagger}}{RT}} \quad (2)$$

Estimating the rate constant $k = 8.3 \times 10^{-8}$ s^{-1} from the reported conversion (0.25) and time (5 weeks) leads to an activation free energy $\Delta G^{\ddagger}$ (473 K) of 180 kJ/mol. This is generally consistent

with the calculated reaction energy at this temperature (ΔG *ca*. 110 kJ/(mol H_2), Table 4) and demonstrates that even seemingly unstable reactions can proceed given sufficient time. However, the principle of microscopic reversibility suggests the reverse reaction will proceed more quickly, $\Delta G^{\ddagger}$ (473 K) ca. 70 kJ/mol, unless the products are somehow prevented from recombining. This was the case in the reported work[7] where the H_2 gas generated was removed under vacuum. Another way the reverse reaction may be impeded is if the solid products become phase– separated so that $Mg(B_3H_8)_2$ and MgH_2 are not in intimate contact. However, this seems unlikely since the $Mg(BH_4)_2$ could be regenerated from the products by increasing the H_2 pressure (120 bar, 523 K, 48 h). Further, the formation of $Mg(B_3H_8)_2$ also takes place in closed reaction vessels where the H_2 generated remains in contact with the reaction mixture. We heated 100 mg of $Mg(BH_4)_2$ in a closed 10 mL vessel at 523 K for 12 h, and dissolved the product in D_2O/THF for analysis by NMR spectroscopy (see SI, section S5). We observed conversion of 20% of the BH_4^- to $B_3H_8^-$, which would generate *ca*. 1 atm H_2 gas inside the reaction vessel. In contrast, the equilibrium partial pressure calculated from the free energy presented in Table 4 is ca. 10^{-12} atm. Consequently, although it is is interesting to note how the Eyring analysis shows that slow formation of unstable species is possible, we do not believe it is the primary reason for the experimental observations of $Mg(B_3H_8)_2$.

B. Fluxional reorientation of the $B_3H_8^-$ anion

Although the $B_3H_8^-$ anion contains two different boron environments, the environment of an individual B atom can switch with relatively small movements of the bridging hydrogens. This can be accomplished by hydrogen rather than boron movements, and has been examined in theoretical studies[37-38] which showed a barrier of only ca. 4 kJ/mol for reorientation of the $B_3H_8^-$ anion. In addition, the entire anion can reorient above 316 K[39] giving rise to a considerable degree of mobility whose entropy is not taken into account in the present DFT calculations.

The mobility is evident in the NMR spectra, which display only one ^{11}B resonance despite the two chemically distinct sites. We calculated chemical shifts of -10.8 ppm for the boron atom connected to two bridged hydrogen atoms, and -40.6 ppm for the two boron atoms each bound to one bridged hydrogen. The weighted average of these resonances, -30.6 ppm, agrees closely with the observed chemical shift,[32] indicating that the boron environments are in rapid exchange over the NMR time

scale. It is apparent that the fluxional rearrangements of $B_3H_8^-$ takes place in the solid state in addition to solution. This has been studied in solid KB_3H_8 where synthetic methods for preparing solvent– free powders have been known for some time.[40] Recent MAS spectra[41] show each polymorph has a single ^{11}B NMR resonance near -30 ppm at room temperature, suggesting that the boron atoms experience the same chemical environment on an NMR time scale. This is in agreement with previous studies at lower field which indicated reorientations of the anion in the crystal lattice[42] and showed a slightly asymmetric singlet for measurements at 30 MHz which became more complex at lower frequencies.[43] The lines narrowed above 316 K when a phase transition to a disordered state occurs, but the room temperature x–ray structure[39, 41] contains the two different boron environments.

Recent inelastic and quasi–elastic neutron measurements[39] have also indicated a surprising degree of motion in KB_3H_8 at temperatures above 200 K. The motion evolves from 3–fold reorientations of $B_3H_8^-$ at low temperature to 4–fold reorientations with a 3 ps relaxation time associated with a phase change above 316 K. Symmetry considerations dictate that the 4–fold reorientation requires movement of boron atoms, and not simply exchange of protons.

It is clear that the entropy associated with this motion will contribute to the stability of $Mg(B_3H_8)_2$, but it is unlikely that it will be sufficient to explain the whole discrepancy between experiment and theory. Our calculations including vibrational, but not fluxional, entropy result in a free energy of formation for $Mg(B_3H_8)_2$ of ca. 100 kJ/(mol H_2) at the observed dehydrogenation temperature (Table 4). The entropy associated with reorientation would therefore need to be ca. 100 J/(K mol $B_3H_8^-$) to offset this. This is approximately the same as the 3–dimensional translational entropy of free H_2 gas, and it is hard to imagine that lattice reorientations could contribute the same amount of entropy.

C. The structure of $Mg(B_3H_8)_2$ in the solid–state

The calculations of energies are based on a theoretically predicted[12] structure for $Mg(B_3H_8)_2$ since there is no experimentally determined one. This may not be the correct description of $Mg(B_3H_8)_2$; indeed calculation of the XRD pattern from this structure does not match the observed pattern published by Moury *et al*.[44] Zhang *et al*.[12] recognized this, and discussed the validity of their

structure and calculations through comparisons with other, structurally characterized, $B_3H_8^-$ compounds. Even if the theoretical structure is not matched by experiment, it seems unlikely that the use of an experimentally–determined structure could lower the reaction free energy sufficiently from the 100 kJ/(mol H_2) we calculated to make $Mg(B_3H_8)_2$ theoretically stable.

Although the calculations are based on crystalline $Mg(B_3H_8)_2$ and MgH_2, *in–situ* diffraction studies[28, 45] show that $Mg(BH_4)_2$ transforms to an amorphous state upon initial dehydrogenation, and that crystalline MgH_2 only forms at higher temperatures, 320–350 °C. The balanced reaction requires that both $B_3H_8^-$ and H^- are formed from dehydrogenation, and these species are likely to be present in an unstructured and somewhat random configuration rather than phase–separating to crystalline products. Kang *et al*.[46] investigated this by considering species ranging between molecular (0D) and crystalline (3D) as condensed phases. Interestingly, they found that dehydrogenation to $Mg(B_3H_8)_2$, MgH_2, and H_2 is energetically favored by ca. 65 kJ/(mol H_2) after including the entropy for H_2 gas at 500 K for 0D condensed phases. This apparent stability is overshadowed by the larger increase in free energy calculated to transform $Mg(BH_4)_2$ from the crystalline 3D state to the 0D state, but it does illustrate how the arrangement of species in the condensed state can have a profound effect on thermodynamics. Although there is some disagreement in the literature, we note that recent work has reported $Mg(BH_4)_2$ melting before dehydrogenation,[45] which corresponds to a transition from a 3D crystal to an amorphous state that approximates a 0D configuration. $Mg(BH_4)_2$ purified with supercritical N_2 was also observed[47] to become amorphous after heating to 300 K, before significant dehydrogenation occurred.

The calculations of Kang *et al*.[46] suggest that the amorphous or 0D nature of $Mg(B_3H_8)_2$ has the greatest influence on its observed stability. Entropy associated with the reorientations of $B_3H_8^-$ is likely to make an additional contribution. We believe that discrepancy between experiment and theory arises from considering $Mg(B_3H_8)_2$ as a discrete compound during the decomposition of $Mg(BH_4)_2$ when the NMR observations are better described as $B_3H_8^-$ anions in an amorphous mixture which also contains BH_4^-, Mg^{2+}, H^- (to balance stoichiometry), and perhaps other anions. The stability of this amorphous mixture is considerably different from discrete $Mg(B_3H_8)_2$ as shown in a recent study.[32] In this work, $Mg(B_3H_8)_2$ began to decompose at 373 K to form BH_4^- and closo–boranes. When mixed with MgH_2, the decomposition was faster and complete conversion to $Mg(BH_4)_2$ was reported at 473 K. The contrast with the *formation* of $B_3H_8^-$ from

$Mg(BH_4)_2$ at the same temperature is stark, and highlights the difference in stability between discrete $Mg(B_3H_8)_2$ and a mixture containing Mg^{2+} and $B_3H_8^-$. This is depicted schematically in Figure 2.

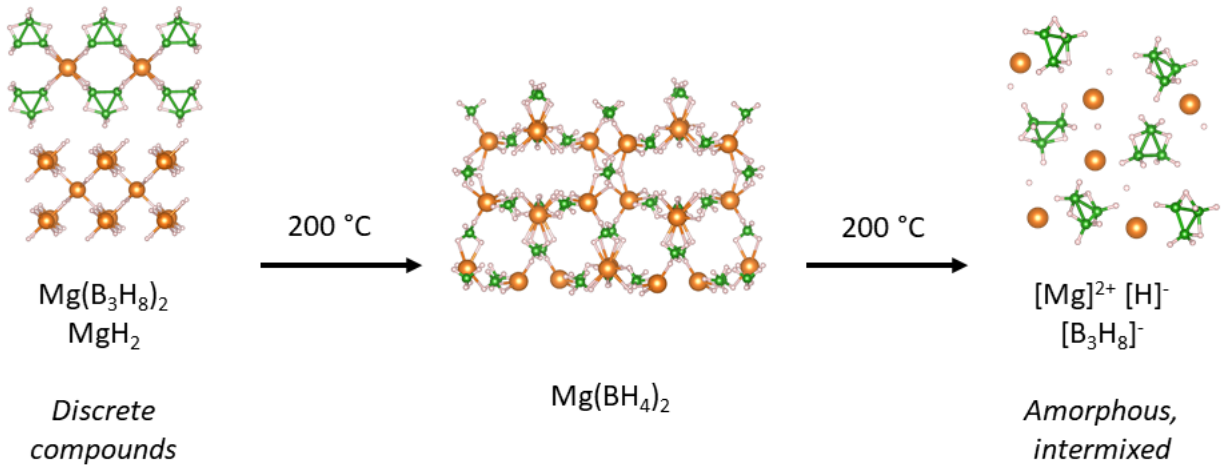

Figure 2: Schematic representation of the difference in reactivity between a coarse-scale mixture of discrete $Mg(B_3H_8)_2$ and MgH_2, and an molecular-scale blend of the ions these compounds are comprised of.

3.5 Dehydrogenation products with favorable thermodynamics

$MgB_{12}H_{12}$ is the only dehydrogenation product we examined which has a negative free energy of reaction (ΔG = -4 kJ/(mol H_2) , Table 3). This, coupled with any kinetic barriers, suggests that a high hydrogen pressure will be required to reverse the reaction to regenerate $Mg(BH_4)_2$, and we are not aware of any successful attempts to rehydrogenate $MgB_{12}H_{12}$. Dehydrogenation to MgB_2H_6, $MgB_{10}H_{10}$, $Mg_3(B_3H_6)_2$ or MgB_2 all have calculated values for ΔH and ΔG that should be reversible assuming kinetic barriers are not extreme. A cycle between $Mg(BH_4)_2$ and MgB_2 delivers the highest hydrogen capacity, however efforts so far have not been able to reduce the temperature for dehydrogenation below around 723 K[5, 48] or the rehydrogenation pressure below 900 bar H_2.[6] $MgB_{10}H_{10}$ (8.2 wt.% H_2, ΔG = 10.2 kJ/(mol H_2)) is a promising target for reversible dehydrogenation, and recent studies[11, 49] have shown that ether addititives, and especially glymes, can direct dehydrogenation to this product. Reversibility remains to be demonstrated, and although phase separation of the MgH_2 co–product may lead to kinetic limitations or reduced capacity over many cycles the thermodynamics suggest it is possible.

MgB_2H_6 and $Mg_3(B_3H_6)_2$ are also interesting targets for dehydrogenation because they have relatively small calculated free energies, ΔG = 21.5 and 9.7 kJ/(mol H_2) respectively, but also because they do not form MgH_2 as a co–product. Avoiding the formation of MgH_2 during H_2 release from $Mg(BH_4)_2$ has two benefits: (i) MgH_2 'parks' usable hydrogen in a stable metal hydride and (ii) minimizing the number of products or phases should result in more efficient regeneration of the BH_4^-. Even though the formation of MgB_2H_6 is predicted by calculations,[12, 50] it has not been unequivocally identified during dehydrogenation or synthesized as a discrete compound. Yang *et al*.[51] reported a powder diffraction pattern matching that calculated from the theoretical MgB_2H_6 structure from a sample dehydogenated at 550 K. A broad NMR resonance at -24.5 ppm attributed to $B_2H_6^{2-}$ was observed in a separate study[9] although the sample was amorphous to x–rays and we have discussed the difference between solution and solid–state NMR chemical shifts for $B_2H_6^{2-}$. NMR resonances and XRD patterns have also been attributed[52-53] to CaB_2H_6 in the dehydrogenation of $Ca(BH_4)_2$, further supporting the possibility that MgB_2H_6 could be a useful target for $Mg(BH_4)_2$ dehydrogenation. Computational studies that look at the activation barrier for these intermediates would be helpful in determining if their formation is feasible.

It is also interesting to consider the formation of $Mg_3(B_3H_6)_2$, a *trianionic* species that has been predicted by computational methods to have thermodynamic enthalpies in the desired narrow window for reversibility and a theoretical yield of 7.4 wt% H_2. (Table 3). To our knowledge there are no reports of any borane cluster compounds with this structure. The calculated ^{11}B NMR chemical shift is -47.2 ppm (Table 2). However, we are cautious about this assignment because as we describe above, there can be some discrepancy between the calculated and observed ^{11}B chemical shift for smaller borane clusters. Further, the calculated chemical shift for solid–state MgB_2H_6 is only 2.4 ppm downfield from $Mg_3(B_3H_6)_2$ (Table 2), which may make difficult to distinguish these compounds. Since the *trianion* species has not been observed, it is feasible that it's formation is kinetically prohibited, even though the thermodynamics are favorable. A potential reaction pathway leading to $Mg_3(B_3H_6)_2$, derived from a retro–synthetic analysis under the reaction conditions, may involve a series of B–H dehydrogenative coupling steps that release hydrogen concomit with B–B bond formation. By this pathway the first product formed would be the $B_2H_6^{2-}$ dianion discussed above. Reaction of this with a further BH_4^- anion could yield the trianion, with each step comprising the formation of a B–B bond and release of H_2:

$$2BH_4^- \Leftrightarrow B_2H_6^{2-} + H_2 \quad (3)$$

$$BH_4^- + B_2H_6^{2-} \Leftrightarrow B_3H_8^{3-} + H_2 \quad (4)$$

$$B_3H_8^{3-} \Leftrightarrow B_3H_6^{3-} + H_2 \quad (5)$$

Formation of $Mg_3(B_3H_6)_2$ would be an attractive end product with the release of 7.5 wt.% H_2 from $Mg(BH_4)_2$ if the reaction pathway is feasible. Further work, outside the current scope of this paper, would be required to calculate the barriers for the dehydrogenative coupling of B–H bonds to gain insight into the kinetic barriers for formation of $B_3H_6^{3-}$.

4. Conclusions

The reaction free energies and solid state ^{11}B NMR chemical shifts of key compounds that may be formed during H_2 release from $Mg(BH_4)_2$ were evaluated using solid–state density functional theory. In many cases we employed supercells containing several formula units, and the results were compared to previously published values. The larger supercells, that are expected to affect the entropic contributions of the soft lattice models, resulted in only minor changes to the calculated energies except for the entropy of reaction to form $Mg(B_3H_8)_2$, which increased from 65.5 to 84.9 kJ/(mol H_2) at 300 K. Although we find that $Mg(B_3H_8)_2$ is slightly more stable than previously predicted, the free energy of reaction was calculated to be 98.5 kJ/(mol H_2) at 600 K, which is still inconsistent with the experimental observation of the $B_3H_8^{2-}$ anion by NMR spectroscopy. We discuss three different possibilities for these discrepancies: the kinetics of formation, the effects of the fluxional reorientation of the $B_3H_8^-$ and alternative solid–state forms of $Mg(B_3H_8)_2$. Careful consideration of experimental evidence suggests that energetically unfavorable products can form in sufficient time even if the activation barrier is high; however that would imply a significantly faster reverse reaction which has not been observed, either here

or in previous experiments.[7-8] Another possibility we considered is the effect of the reorientation of $B_3H_8^-$ anion, due to both hydrogen transfer between the borons and overall reorientation, that results in significant dynamics observed in NMR studies and classic inelastic and quasi–elastic neutron measurements.[39] The entropy associated with this fluxional behavior is not captured within the harmonic approximation in the DFT calculations, and is not accounted for in the thermochemical analysis. However, the additional entropy would need to be *ca*. 100 J/(K mol $B_3H_8^-$) to bring the calculated free energy close to equilibrium, and it is unlikely that lattice reorientations could contribute this amount of entropy. We propose that the major reason for the discrepancy is that the calculations consider the products to be separate crystalline phases of $Mg(B_3H_8)_2$ and MgH_2, whereas the experimental observation is an amorphous material likely to contain a random assemblage of Mg^{2+}, $B_3H_8^{2-}$, and H^- in an intimate mixture. This is supported by a number of experimental measurments: primarly the inconsistency between the XRD pattern calculated for the proposed structure and the one published by Moury *et al*.,[44] and the observations of an amorphous product which also contains other anions (BH_4^-, Mg^{2+}, H^-) rather than crystalline $Mg(B_3H_8)_2$. Computationally, Kang *et al*.[46] showed that the thermochemistry of the reaction changes very significantly with reduced ordering of $Mg(B_3H_8)_2$ from a 3D crystal to a 0D amorphous state. To this end, more sophisticated computational models that can account for lower dimensionality or amorphous structures will be critical to enable researchers to predict suitable intermediates in complex hydrides that have both the proper thermodynamics and kinetics for reversible cycling to store hydrogen.

Even though $MgB_{10}H_{10}$ and $MgB_{12}H_{12}$ have received most attention as promising targets for reversible dehydrogenation, the calculated ^{11}B NMR chemical shifts should prove valuable for identifying other intermediates and products in future studies. Amongst these, MgB_2H_6 and

$Mg_3(B_3H_6)_2$ make interesting new targets for dehydrogenation of $Mg(BH_4)_2$ with relatively low enthalpies and no formation of hydride, which may be beneficial in releasing more H_2 and avoiding the formation of phase separated products. Both of these factors should assist in rehydrogenation to make a reversible system for hydrogen storage.

5. Acknowledgements

Research support from the Hydrogen Materials - Advanced Research Consortium (HyMARC), established as part of the Energy Materials Network under the U.S. Department of Energy, Office of Energy Efficiency and Renewable Energy, Fuel Cell Technologies Office is gratefully acknowledge. The authors thank Craig Jensen, Brandon Wood and Ned Stetson for insightful discussion. All of the quantum chemical calculations were performed at EMSL (grid.436923.9), a DOE Office of Science User Facility sponsored by the Biological and Environmental Research program and located at Pacific Northwest National Laboratory (PNNL). PNNL is a multi-program national laboratory operated by Battelle for the U.S. Department of Energy under Contract DE-AC05-76RL01830

6. Supporting Information

The following has been provided as a Supporting Information to this manuscript: detailed descriptions of the theoretical approaches used in the calculations of the thermochemistry and the NMR chamical shifts; visual representation of the gas-phase optimized molecular models and tables of their NMR shits; and report of the NMR measurments for dehadrogentaion of $Mg(BH_4)_2$ in a closed reaction vessel.

7. References

1. Arbabzadeh, Maryam; Ramteen Sioshansi; Jeremiah X. Johnson; Gregory A. Keoleian, The role of energy storage in deep decarbonization of electricity production. *Nature Communications* **2019,** *10* (1), 3413.
2. Pivovar, Bryan; Neha Rustagi; Sunita Satyapal, Hydrogen at Scale (H 2 @Scale): Key to a Clean, Economic, and Sustainable Energy System. *The Electrochemical Society Interface* **2018,** *27* (1), 47-52.
3. Stetson, Ned; Marika Wieliczko, Hydrogen technologies for energy storage: A perspective. *MRS Energy & Sustainability* **2020,** *7* (1), 41.
4. Ozolins, V.; E. H. Majzoub; C. Wolverton, First-principles prediction of thermodynamically reversible hydrogen storage reactions in the Li-Mg-Ca-B-H system. *J Am Chem Soc* **2009,** *131* (1), 230-237.
5. Soloveichik, G. L.; Y. Gao; J. Rijssenbeek; M. Andrus; S. Kniajanski; R. C. Bowman; S. J. Hwan; J. C. Zhao, Magnesium borohydride as a hydrogen storage material: Properties and dehydrogenation pathway of unsolvated $Mg(BH_4)_2$. *International Journal of Hydrogen Energy* **2009,** *34* (2), 916-928.
6. Severa, G.; E. Ronnebro; C. M. Jensen, Direct hydrogenation of magnesium boride to magnesium borohydride: demonstration of > 11 weight percent reversible hydrogen storage. *Chemical Communications* **2010,** *46* (3), 421-423.
7. Chong, M.; A. Karkamkar; T. Autrey; S. Orimo; S. Jalisatgi; C. M. Jensen, Reversible dehydrogenation of magnesium borohydride to magnesium triborane in the solid state under moderate conditions. *Chemical Communications* **2011,** *47* (4), 1330-1332.
8. Chong, M.; Motoaki, M,; Orimo,S.; Autrey, T.; Jensen, C.M. Selective Reversible Hydrogenation of $Mg(B_3H_8)_2/MgH_2$ to $Mg(BH_4)_2$: Pathway to Reversible Borane-Based Hydrogen Storage? *Inorganic Chemistry* **2015,** *54* (8), 4120-4125.
9. Yan, Yigang; Hai-Wen Li; Hideki Maekawa; Masakazu Aoki; Tatsuo Noritake; Mitsuru Matsumoto; Kazutoshi Miwa; Shin-ichi Towata; Shin-ichi Orimo, Formation Process of $[B_{12}H_{12}]^{2-}$ from $[BH_4]^-$during - the Dehydrogenation Reaction of $Mg(BH_4)_2$. *MATERIALS TRANSACTIONS* **2011,** *52* (7), 1443-1446.
10. Saldan, Ivan, Decomposition and formation of magnesium borohydride. *International Journal of Hydrogen Energy* **2016,** *41* (26), 11201-11224.
11. Chong, M.; Autrey, T.; Jensen, C.M. Lewis Base Complexes of Magnesium Borohydride: Enhanced Kinetics and Product Selectivity upon Hydrogen Release. *Inorganics* **2017,** *5* (4).
12. Zhang, Y. S.; E. Majzoub; V. Ozolins; C. Wolverton, Theoretical prediction of metastable Intermediates in the decomposition of $Mg(BH_4)_2$. *Journal of Physical Chemistry C* **2012,** *116* (19), 10522-10528.
13. Alapati, S. V.; J. K. Johnson; D. S. Sholl, Using first principles calculations to identify new destabilized metal hydride reactions for reversible hydrogen storage. *Physical Chemistry Chemical Physics* **2007,** *9* (12), 1438-1452.
14. Kim, K. C.; A. D. Kulkarni; J. K. Johnson; D. S. Sholl, Examining the robustness of first-principles calculations for metal hydride reaction thermodynamics by detection of metastable reaction pathways. *Physical Chemistry Chemical Physics* **2011,** *13* (48), 21520-21529.
15. Kim, K. C.; A. D. Kulkarni; J. K. Johnson; D. S. Sholl, Large-scale screening of metal hydrides for hydrogen storage from first-principles calculations based on equilibrium reaction thermodynamics. *Physical Chemistry Chemical Physics* **2011,** *13* (15), 7218-7229.
16. Kresse, G.; J. Furthmuller, Efficient iterative schemes for ab initio total-energy calculations using a plane-wave basis set. *Physical Review B* **1996,** *54* (16), 11169-11186.

17. Perdew, J. P.; K. Burke; M. Ernzerhof, Generalized gradient approximation made simple. *Physical Review Letters* **1996,** *77* (18), 3865-3868.
18. Perdew, J. P.; K. Burke; M. Ernzerhof, Generalized gradient approximation made simple (vol 77, pg 3865, 1996). *Physical Review Letters* **1997,** *78* (7), 1396-1396.
19. Blochl, P. E., Projector augmrnted-wave method. *Physical Review B* **1994,** *50* (24), 17953-17979.
20. Togo, A.; Tanaka, I. First principles phonon calculations in materials science. *Scripta Materialia* **2015,** *108*, 1-5.
21. Aprà, E.; E. J. Bylaska; W. A. de Jong; N. Govind; K. Kowalski; T. P. Straatsma; M. Valiev; H. J. J. van Dam; Y. Alexeev; J. Anchell; V. Anisimov; F. W. Aquino; R. Atta-Fynn; J. Autschbach; N. P. Bauman; J. C. Becca; D. E. Bernholdt; K. Bhaskaran-Nair; S. Bogatko; P. Borowski; J. Boschen; J. Brabec; A. Bruner; E. Cauët; Y. Chen; G. N. Chuev; C. J. Cramer; J. Daily; M. J. O. Deegan; T. H. DunningJr.; M. Dupuis; K. G. Dyall; G. I. Fann; S. A. Fischer; A. Fonari; H. Früchtl; L. Gagliardi; J. Garza; N. Gawande; S. Ghosh; K. Glaesemann; A. W. Götz; J. Hammond; V. Helms; E. D. Hermes; K. Hirao; S. Hirata; M. Jacquelin; L. Jensen; B. G. Johnson; H. Jónsson; R. A. Kendall; M. Klemm; R. Kobayashi; V. Konkov; S. Krishnamoorthy; M. Krishnan; Z. Lin; R. D. Lins; R. J. Littlefield; A. J. Logsdail; K. Lopata; W. Ma; A. V. Marenich; J. Martin del Campo; D. Mejia-Rodriguez; J. E. Moore; J. M. Mullin; T. Nakajima; D. R. Nascimento; J. A. Nichols; P. J. Nichols; J. Nieplocha; A. Otero-de-la-Roza; B. Palmer; A. Panyala; T. Pirojsirikul; B. Peng; R. Peverati; J. Pittner; L. Pollack; R. M. Richard; P. Sadayappan; G. C. Schatz; W. A. Shelton; D. W. Silverstein; D. M. A. Smith; T. A. Soares; D. Song; M. Swart; H. L. Taylor; G. S. Thomas; V. Tipparaju; D. G. Truhlar; K. Tsemekhman; T. Van Voorhis; Á. Vázquez-Mayagoitia; P. Verma; O. Villa; A. Vishnu; K. D. Vogiatzis; D. Wang; J. H. Weare; M. J. Williamson; T. L. Windus; K. Woliński; A. T. Wong; Q. Wu; C. Yang; Q. Yu; M. Zacharias; Z. Zhang; Y. Zhao; R. J. Harrison, NWChem: Past, present, and future. *The Journal of Chemical Physics* **2020,** *152* (18), 184102.
22. Momma, K.; Izumi, F. VESTA 3 for three-dimensional visualization of crystal, volumetric and morphology data. *Journal of Applied Crystallography* **2011,** *44* (6), 1272-1276.
23. Filinchuk, Y.; Černý, R.; Hagemann, H. Insight into $Mg(BH_4)_2$ with Synchrotron X-ray Diffraction: Structure Revision, Crystal Chemistry, and Anomalous Thermal Expansion. *Chemistry of Materials* **2009,** *21* (5), 925-933.
24. Her, J.; Stephens, P.W.; Gao,Y.; Soloveichik, G.L.; Rijssenbeek, J.; Andrus, M.; Zhao, J. Structure of unsolvated magnesium borohydride $Mg(BH_4)_2$. *Acta Crystallographica Section B* **2007,** *63* (4), 561-568.
25. Filinchuk, Y.; B. Richter; T. R. Jensen; V. Dmitriev; D. Chernyshov; H. Hagemann, Porous and dense magnesium borohydride frameworks: Synthesis, stability, and reversible absorption of guest species. *Angewandte Chemie-International Edition* **2011,** *50* (47), 11162-11166.
26. Ozolins, V.; E. H. Majzoub; C. Wolverton, First-principles prediction of a ground state crystal structure of magnesium borohydride. *Physical Review Letters* **2008,** *100* (13), 230-237.
27. Majzoub, E. H.; V. Ozoliņš, Prototype electrostatic ground state approach to predicting crystal structures of ionic compounds: Application to hydrogen storage materials. *Physical Review B* **2008,** *77* (10), 104115.
28. David, W. I. F.; S. K. Callear; M. O. Jones; P. C. Aeberhard; S. D. Culligan; A. H. Pohl; S. R. Johnson; K. R. Ryan; J. E. Parker; P. P. Edwards; C. J. Nuttall; A. Amieiro-Fonseca, The structure, thermal properties and phase transformations of the cubic polymorph of magnesium tetrahydroborate. *Physical Chemistry Chemical Physics* **2012,** *14* (33), 11800-11807.

29. Bil, A.; B. Kolb; R. Atkinson; D. G. Pettifor; T. Thonhauser; A. N. Kolmogorov, van der Waals interactions in the ground state of $Mg(BH_4)_2$ from density functional theory. *Physical Review B* **2011,** *83* (22), 224103.
30. Dai, B.; Sholl, D. S.; Johnson, J. K. First-Principles Study of Experimental and Hypothetical $Mg(BH_4)_2$ Crystal Structures. *The Journal of Physical Chemistry C* **2008,** *112* (11), 4391-4395.
31. Pinatel, E. R.; E. Albanese; B. Civalleri; M. Baricco, Thermodynamic modelling of $Mg(BH_4)_2$. *Journal of Alloys and Compounds* **2015,** *645*, S64-S68.
32. Gigante, A.; Leick, N.; Lipton, A.S.; Tran, B.; Strange N. A.; Bowden, M.;. Martinez M. B; Moury R.; Gennett, T.; Hagemann, H; Autrey, T. S. Thermal Conversion of Unsolvated $Mg(B_3H_8)_2$ to BH_4^- in the Presence of MgH_2. *ACS Applied Energy Materials* **2021,** *4* (4), 3737-3747.
33. Hosmane, N. S.; Wermer, J. R.; Hong, Z; Getman, T. D.; Shore, S. G. High yield preparation of the tetradecahydroundecaborate(1-) anion, $[B_{11}H_{14}]^-$, from pentaborane(9). *Inorganic Chemistry* **1987,** *26* (21), 3638-3639.
34. Godfroid, R. A.; Hill,T. G.; Onak, T. P.; Shore, S. G. Formation of $[BH_3]^{2-}$ and $[B_2H_6]^{2-}$ From the Homogeneous Reduction of B_2H_6. *Journal of the American Chemical Society* **1994,** *116* (26), 12107-12108.
35. Hwang, S. J.; R. C. Bowman; J. W. Reiter; J. Rijssenbeek; G. L. Soloveichik; J. C. Zhao; H. Kabbour; C. C. Ahn, NMR confirmation for formation of $[B_{12}H_{12}]^{2-}$ complexes during hydrogen desorption from metal borohydrides. *Journal of Physical Chemistry C* **2008,** *112* (9), 3164-3169.
36. Li, H. W.; K. Kikuchi; Y. Nakamori; N. Ohba; K. Miwa; S. Towata; S. Orimo, Dehydriding and rehydriding processes of well-crystallized $Mg(BH_4)_2$ accompanying with formation of intermediate compounds. *Acta Materialia* **2008,** *56* (6), 1342-1347.
37. Pepperberg, I. M.; D. A. Dixon; W. N. Lipscomb; T. A. Halgren, The question of fluxional behavior in octahydrotriborate(1-) and pentaborane(11). *Inorganic Chemistry* **1978,** *17* (3), 587-593.
38. Olson, J. K.; Boldyrev. A. I. Ab initio characterization of the flexural $B_3H_8^-$ anion found in the reversible dehydrogenation. *Computational and Theoretical Chemistry* **2011,** *967* (1), 1-4.
39. Andersson, M. S.; J. B. Grinderslev; X. M. Chen; X. Chen; U. Häussermann; W. Zhou; T. R. Jensen; M. Karlsson; T. J. Udovic, Interplay between the reorientational dynamics of the $B_3H_8^-$ anion and the structure in KB_3H_8. *The Journal of Physical Chemistry C* **2021,** *125* (7), 3716-3724.
40. Hill, T. G.; Godfroid, R. A.; White, J. P.; Shore, S. G. Reduction of borane THF by alkali metal (potassium, rubidium, cesium) and ytterbium mercury amalgams to form salts of octahydrotriborate(1-); a simple procedure for the synthesis of tetraborane(10). *Inorganic Chemistry* **1991,** *30* (14), 2952-2954.
41. Grinderslev, J. B.; Møller, K. T.; Yan, Y.; Chen, X.; Li, Y.; Li, H.; Zhou, W.; Skibsted, J.; Chen, X.; Jensen, T. R. Potassium octahydridotriborate: diverse polymorphism in a potential hydrogen storage material and potassium ion conductor. *Dalton Transactions* **2019,** *48* (24), 8872-8881.
42. Reynhardt, E. C.; J. A. J. Lourens, NMR study of proton and boron dynamics in KB_3H_8. *Journal of Physics C: Solid State Physics* **1980,** *13* (14), 2765-2779.
43. Paine, R. T.; Eiichi Fukushima; S. B. W. Roeder, Structure and hindered motion of B_3H_8 anions in solids: An NMR study. *Chemical Physics Letters* **1975,** *32* (3), 566-568.

44. Moury, R. ; Gigante, A.; Remhof, A.; Roedern, E.; Hagemann, H. Experimental investigation of $Mg(B_3H_8)_2$ dimensionality, materials for energy storage applications. *Dalton Transactions* **2020,** *49* (35), 12168-12173.
45. Paskevicius, M; Pitt, M. P.; Webb, C. J.; Sheppard, D.A.; Filsø, U.; Gray, E. M.; Buckley, C. E., In-situ x-ray diffraction study of γ-$Mg(BH_4)_2$ decomposition. *The Journal of Physical Chemistry C* **2012,** *116* (29), 15231-15240.
46. Kang, S.; Heo, T.W.; Allendorf, M. D. ; Wood. B. C. Morphology-Dependent Stability of Complex Metal Hydrides and Their Intermediates Using First-Principles Calculations. *ChemPhysChem* **2019,** *20* (10), 1340-1347.
47. Stadie, N. P.; Callini, E.; Richter, B.; Jensen, T. R.; Borgschulte, A.; Züttel, A. Supercritical N_2 Processing as a Route to the Clean Dehydrogenation of Porous $Mg(BH_4)_2$. *Journal of the American Chemical Society* **2014,** *136* (23), 8181-8184.
48. Newhouse, R. J.; Stavila, V.; Hwang, S. ; Klebanoff, L. E.; Zhang, J. Z. Reversibility and improved hydrogen release of magnesium borohydride. *The Journal of Physical Chemistry C* **2010,** *114* (11), 5224-5232.
49. Tran, B. L.; Allen, T. N.; Bowden, M.E.; Autrey, T.; Jensen,C.M. Effects of Glymes on the Distribution of $Mg(B_{10}H_{10})$ and $Mg(B_{12}H_{12})$ from the Thermolysis of $Mg(BH_4)_2$. *Inorganics* **2021,** *9* (6), 41.
50. van Setten, M. J.; W. Lohstroh; M. Fichtner, A new phase in the decomposition of $Mg(BH_4)_2$: first-principles simulated annealing. *Journal of Materials Chemistry* **2009,** *19* (38), 7081-7087.
51. Yang, J; Zhang, X.; Zheng, J.; Song, P.; Li, X. Decomposition pathway of $Mg(BH_4)_2$ under pressure: Metastable phases and thermodynamic parameters. *Scripta Materialia* **2011,** *64* (3), 225-228.
52. Yan, Y.; Remhof, A.; Rentsch, D.; Züttel, A.; Giri, S; Jena, P. A novel strategy for reversible hydrogen storage in $Ca(BH_4)_2$. *Chemical Communications* **2015,** *51* (55), 11008-11011.
53. Yan, Y.; Rentsch, D.; Remhof, A. Controllable decomposition of $Ca(BH_4)_2$ for reversible hydrogen storage. *Physical Chemistry Chemical Physics* **2017,** *19* (11), 7788-7792.

TOC graphic

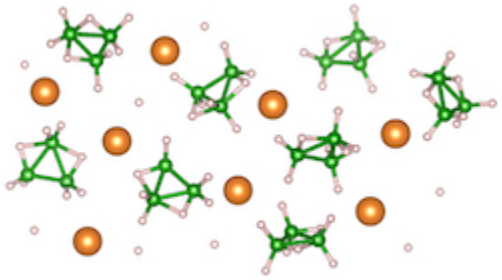

Analysis of Intermediates and Products from the Dehydrogenation of $Mg(BH_4)_2$

Iffat H. Nayyar[1], Bojana Ginovska[1], Mark Bowden*[1], Gary Edvenson[2], Ba Tran[1] and Tom Autrey[1]*

[1]Physical Sciences Division, Physical and Computational Sciences Directorate, Pacific Northwest National Laboratory, Richland, WA 99354, USA

[2]Chemistry & Biochemistry Department, Minnesota State University, Moorhead, MN 56563

*Corresponding authors: bojana.ginovska@pnnl.gov; mark.bowden@pnnl.gov

Supporting Information

Table of Contents

S1. Thermodynamic calculation method **2**

S2. NMR chemical shift calculation method **4**

S3. DFT and NMR calculations of the gas–phase species **6**

S4. Gas–phase optimized molecular models and NMR shifts **6**

S5. Dehydrogenation of $Mg(BH_4)_2$ in a closed reaction vessel **10**

References **11**

S1. Thermodynamic calculation method

In the present approach, the stability of a broad class of complex metal hydrides is investigated by calculating the enthalpy of reaction and parameters for reaction equilibrium for the decomposition of magnesium borohydride into borane compounds accompanied by the release of hydrogen. All borohydrides are represented as infinite solids in the crystalline state. The temperature–dependent free energy G of each solid can be written as:[1]

$$G(T) = U - T\,S + P\,V \simeq E + \delta H - t\,S + P\,V = H - T\,S + P\,V \quad \text{(S1)}$$

The first term on the right–hand side is the electronic total energy of the material as computed using density functional theory (DFT). The vibrational contributions to the internal energy δH and entropy S can be computed within the harmonic approximation once the phonon densities of states for the material are computed.[1-2] Here, we neglect the translational and rotational contributions to the internal energy of the H_2 gas as the zero–point energy calculated with the vibrational frequency was shown to be in good agreement with the experimental value.[2-3] Because the volume change associated with generating gaseous H_2 is large relative to the volume changes in the solid components, PV contributions due to changes in the volumes of the solid phases are neglected. Thus, the reaction free energy is computed as:

$$\Delta G(T) = \Delta H - T\,\Delta S \quad \text{(S2)}$$

The equilibrium pressure P is then given by the van't Hoff equation[2, 4] for the overall reaction:

$$\ln P = -\frac{\Delta H}{RT} + \frac{\Delta S}{R} = -\frac{\Delta G(T)}{R} \quad \text{(S3)}$$

Plane wave DFT calculations were carried out using the Vienna *ab–initio* simulation package (VASP) code[5] with the projector augmented wave (PAW) scheme[6] combined with the ultrasoft pseudopotentials to account for the valence electrons–core interactions. Electron exchange and correlation effects were described using the pure generalized gradient approximation (GGA) method with the PBE functional having no Hartree–Fock mixing.[7-8] These calculations examined crystal structures using periodic boundary conditions in all the principal axes directions. The crystal lattices for all borohydride (MB_xH_y) species under consideration were predicted using the prototype electrostatic ground state (*PEGS*) search methods superseded by *Monte Carlo* based annealing and density functional simulations, as described in detail elsewhere.[9] All atomic positions and cell parameters were relaxed until the forces and stress on each of the unconstrained atoms were below 0.01 eV/Å and 0.2 kbar, respectively. The plane–wave basis with an 875 eV cutoff and a Monkhorst–Pack grid of 36 *k*–points were used. The choice of *k*–points has yielded energies converged to more than 10^{-6} eV/f.u. The $3s^2$, $3s^1$ and $2s^2\ 2p^1$ were treated as valence electrons for Mg, Na and B respectively.

Calculations of the phonon density of states and the resulting vibrational contributions to the static energy were performed by the linear response Γ–centered analytic second derivative density functional perturbation theory (DFPT) using VASP. [5] Zero–point enthalpies and entropies were obtained by directly summing over all the calculated phonon frequencies. It is necessary to use a relatively large supercell to avoid interactions between images of the displaced atoms when defining their phonon density of states.[1] Finite temperature effects were investigated using the Phonopy code.[10] The code invokes the components from the hessian force constant matrices calculated by DFPT scheme and computes the vibrational and quasi–harmonic thermal corrections

to the energies. Thermal corrections were calculated for temperature range of 0–1000 K. The supercells for higher dimensions were also generated using the same code.

S2. NMR chemical shift calculation method

DFT calculations have proven to be effective in predicting the NMR chemical shifts of a range of known intermediates and are useful for the assignment of unidentified spectral resonances within finite periodic systems. For example, Mauri *et al*.[11-12] benchmarked an NMR calculation method for extended periodic systems using an all–electron Hamiltonian implementation with norm–conserving pseudopotentials. Pickard *et al*.[13] validated the calculations for the NMR chemical shielding using an extended gauge–including GIPAW all–electron method within the Vanderbilt's ultrasoft pseudopotential scheme, which allowed to reconstruct the valence wavefunction in the core region retaining their correct nodal structures.

Alternately, we carried out calculation of chemical shielding tensors for NMR predictions within the framework of the converse approach by Thonhauser *et al*.,[14] as implemented in the VASP code.[5, 15-16] In this approach, the induced magnetic field in response to a uniformly applied field within a linear response framework is calculated by the expression given below; where the shielding tensor $\sigma_{s,\alpha\beta}$ for a particular nucleus s is obtained from the total induced orbital magnetization M^{ind} by a magnetic dipole m_s.[17]

$$\sigma_{s,\alpha\beta} = -\Omega \frac{\partial M_{\beta}^{ind}}{\partial m_{s,\alpha}} \tag{S4}$$

Here α and β are the Cartesian components and Ω the unit cell volume. Henceforth, the elemental isotropic chemical shielding for any defined system is given by the trace of its chemical shielding tensor.[17-18]

$$\sigma_{iso} = \frac{1}{3}(\sigma_{xx} + \sigma_{yy} + \sigma_{zz}) = \frac{1}{3}\, Tr[\boldsymbol{\sigma}] \quad \text{(S5)}$$

The chemical shielding tensor for every atom in the crystal structure of the magnesium borohydride systems under study were calculated using DFT, the GGA functional PBE[8] and PAW potentials,[6] as implemented in the VASP code.[5] The calculated isotropic chemical shift δ_{iso} and absolute chemical shielding σ_{iso} is related through an experimentally measured shielding reference σ_{ref}. [19]

$$\delta_{iso} \approx \sigma_{iso} - \sigma_{ref}\ when\ |\sigma_{ref}| \ll 1 \quad \text{(S6)}$$

All experimentally measured ^{11}B chemical shifts were referenced to boron trifluoride etherate ($BF_3 \bullet Et_2O$). The calculated chemical shifts were reported using the same reference. However, since $BF_3 \bullet Et_2O$ does not exist in the solid–state form under experimental conditions considered, we have chosen the tetragonal–phase $NaBH_4$ [20] as the intermediate reference with the experimentally known ^{11}B chemical shift of –41.6 ppm as referenced to $BF_3 \bullet Et_2O$.[21 22,20]

S3. DFT and NMR calculations of the gas–phase species

All calculations were done using the NWChem software packet.[23] Geometries were optimized using DFT with the B3LYP hybrid functional,[24-25] and all gaussian 6-31+G* basis set.[26] Minima were confirmed as having no imaginary frequencies, calculated in the rigid–rotor, harmonic–oscillator approximation. The ^{11}B chemical shifts were referenced to gas phase optimized boron trifluoride ($BF_3 \bullet Et_2O$).

S4. Gas–phase optimized molecular models and NMR shifts

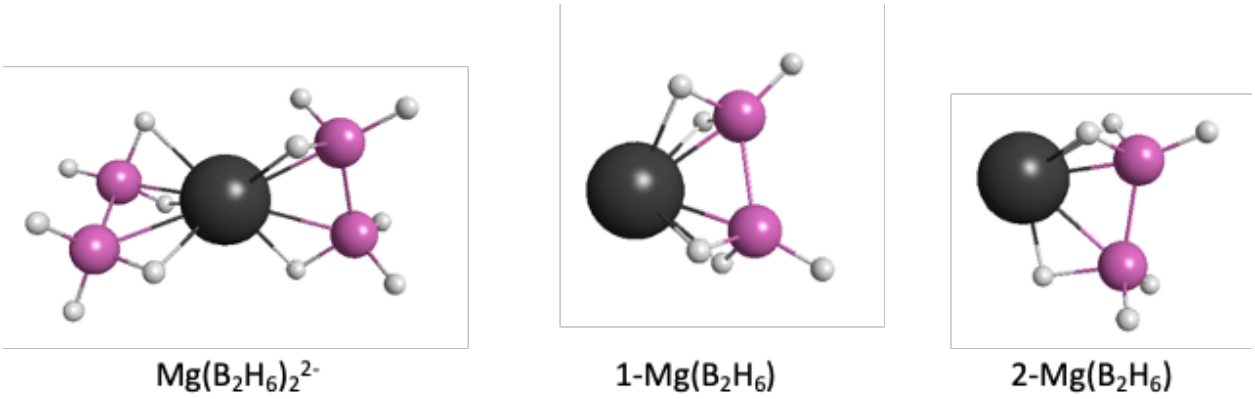

Figure S1: Optimized gas phase geometries for complexes of Mg^{2+} and $B_2H_6^{2-}$. These are the only stable configurations determined by the optimization, using numerous starting configurations. Boron is represented as pink spheres, magnesium as black sphere, and hydrogen as white spheres.

Table S1: Calculated gas–phase ^{11}B NMR chemical shifts for the stable conformations of Mg^{2+} and $B_2H_6^{2-}$ shown in Figure S1, reported relative to $BF_3 \bullet Et_2O$. The subscripts in the column headings refer to chemically distinct boron atoms.

Configuration	$^{11}B_1$ δ (ppm)	$^{11}B_2$ δ (ppm)	$^{11}B_{avg}$ δ (ppm)
1-Mg(B_2H_6)	-14.2		-14.2
2-Mg(B_2H_6)	15.4	-31.1	-7.8
$Mg(B_2H_6)_2^{2-}$	-47.6	-43.3	-45.5
Average			-26.7

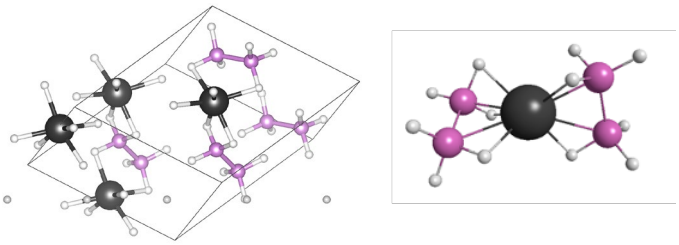

Figure S2. Crystal structure of solid-state MgB_2H_6 (left; B is pink, Mg is gray and H is white) and gas phase optimized structure for $Mg(B_2H_6)_2^{2-}$, showing similarities in the coordination of the boron environments, that gives rise to very similar ^{11}B chemical shifts in the NMR calculations.

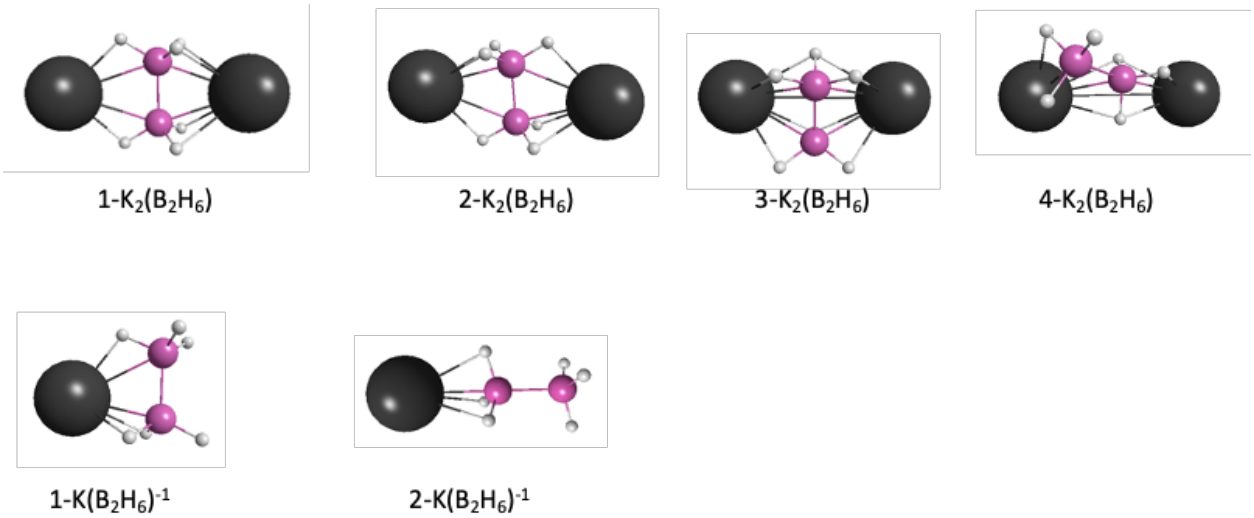

Figure S3. Optimized gas phase geometries for complexes of K^+ and $B_2H_6^{2-}$. These are the only stable configurations determined by the optimization, using numerous starting configurations. Boron is represented as pink spheres, potassium as black sphere, and hydrogen as white spheres.

Table S2: Calculated gas–phase ^{11}B NMR chemical shifts for the stable conformations of K^+ and $B_2H_6^{2-}$ shown in Figure S3, reported relative to $BF_3 \bullet Et_2O$. The subscripts in the column headings refer to chemically distinct boron atoms.

Configuration	**$^{11}B_1$ δ (ppm)**	**$^{11}B_2$ δ (ppm)**	**$^{11}B_{avg}$ δ (ppm)**
1-$K_2(B_2H_6)$	**-37.4**		**-37.4**
2-$K_2(B_2H_6)$	**-33.2**		**-33.2**
3-$K_2(B_2H_6)$	**-33.9**		**-33.9**
4-$K_2(B_2H_6)$	**-33.4**	**-41.2**	**-37.3**
1-$K(B_2H_6)^{-1}$	**-11.1**	**-26.2**	**-18.7**
2-$K(B_2H_6)^{-1}$	**10.6**	**-36.4**	**-12.9**
Average			**-28.9**

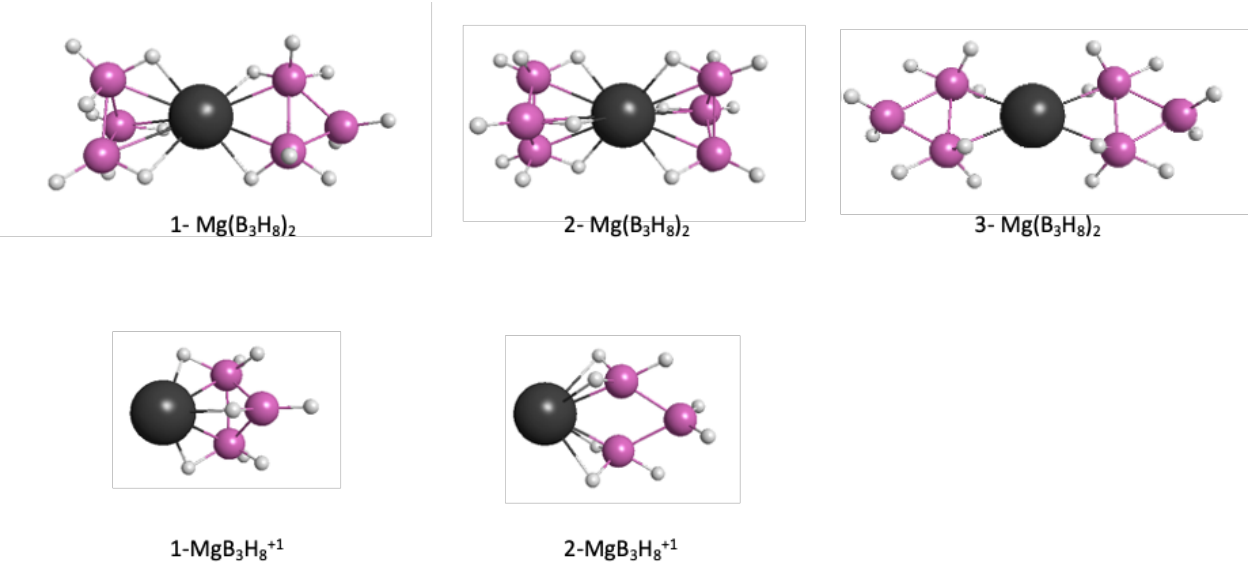

Figure S4: Optimized gas phase geometries for complexes of Mg^{2+} and $B_3H_8^-$. These are the only stable configurations determined by the optimization, using numerous starting configurations. Boron is represented as pink spheres, magnesium as black sphere, and hydrogen as white spheres.

Table S3: Calculated gas–phase ^{11}B NMR chemical shifts for the stable conformations of Mg^{2+} and $B_3H_8^-$ shown in Figure S4, reported relative to $BF_3 \bullet Et_2O$. The subscripts in the column headings refer to chemically distinct boron atoms

Configuration	**$^{11}B_1$ δ (ppm)**	**$^{11}B_2$ δ (ppm)**	**$^{11}B_3$ δ (ppm)**	**$^{11}B_4$ δ (ppm)**	**$^{11}B_{avg}$ δ (ppm)**
1- $Mg(B_3H_8)_2$	**-50.5**	**-13.5**	**-50.6**	**-17.1**	**-33.0**
2- $Mg(B_3H_8)_2$	**-16.3**	**-50.0**			**-33.2**
3- $Mg(B_3H_8)_2$	**-50.5**	**-5.3**			**-27.2**
1-$MgB_3H_8^{+1}$	**-45.5**	**-12.2**			**-28.9**
2-$MgB_3H_8^{+1}$	**-52.5**	**-1.9**			**-27.2**
Average					**-30.0**

S5. Dehydrogenation of $Mg(BH_4)_2$ in a closed reaction vessel

In a glovebox, 100 mg of $Mg(BH_4)_2$ (Aldrich) were loaded into a calorimetry cell (C80, Setaram KEP Technologies) with a volume of 10 mL and closed under an atmosphere of nitrogen gas. The cell was placed in the calorimeter and heated to 250 °C for 12 hours and cooled to room temperature. The solid was dissolved in a mixture of 2:D_2O:1THF and the ^{11}B spectrum recorded at 160 MHz using a Varian NMR spectrometer (Figure 5S).

Most of the boron remained as BH_4^- (-41 ppm) with 21.5% evident as $B_3H_8^-$ (-30 ppm) and a minor amount unidentified at -12 ppm. The hydrogen pressure inside the vessel at the reaction temperature was calculated using this conversion and the ideal gas law as 1.1 atm H_2.

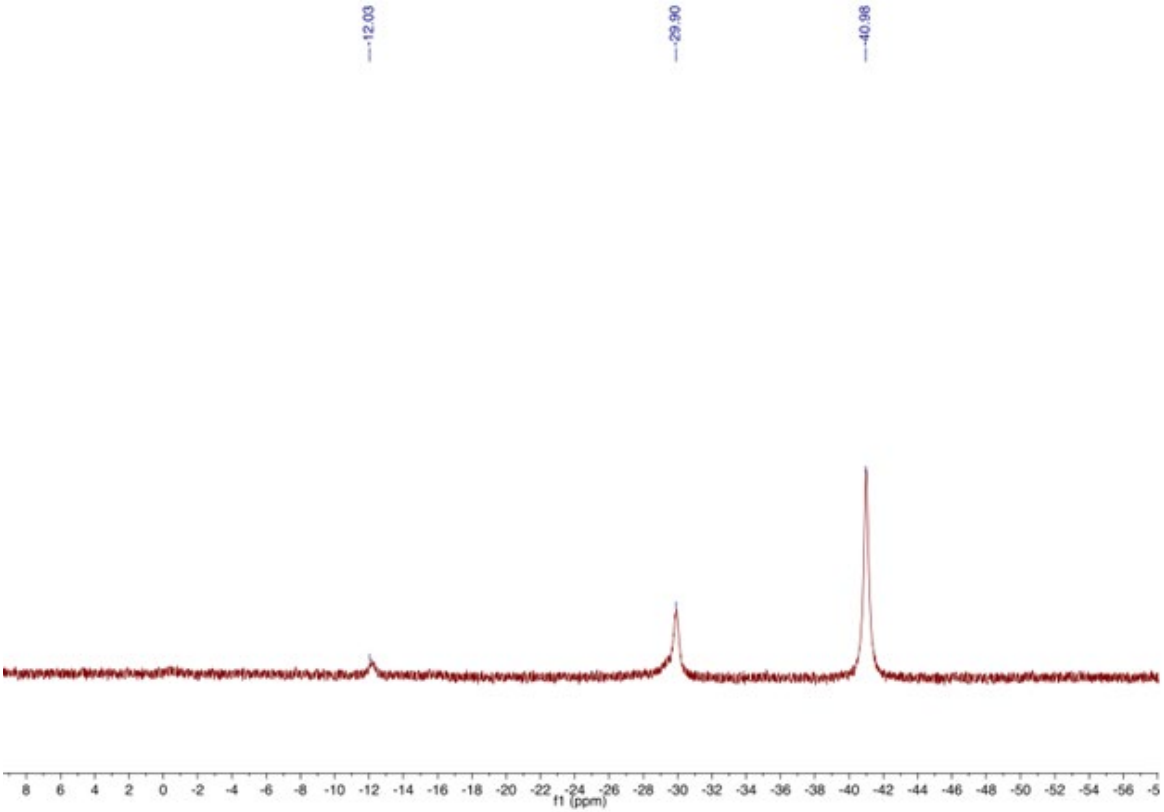

Figure S5. ^{11}B solution NMR spectrum of product obtained after heating $Mg(BH_4)_2$ at 250 °C for 12 hours in a closed vessel.

References

1. Ackland, G. J., Calculation of free energies from ab initio calculation. *Journal of Physics-Condensed Matter* **2002,** *14* (11), 2975-3000.
2. Alapati, S. V.; J. K. Johnson; D. S. Sholl, Using first principles calculations to identify new destabilized metal hydride reactions for reversible hydrogen storage. *Physical Chemistry Chemical Physics* **2007,** *9* (12), 1438-1452.
3. Gross, A.; M. Scheffler, Role of zero-point effects in catalytic reactions involving hydrogen. *Journal of Vacuum Science & Technology a-Vacuum Surfaces and Films* **1997,** *15* (3), 1624-1629.
4. Qiu, C.; S. M. Opalka; G. B. Olson; D. L. Anton, The Na-H system: from first-principles calculations to thermodynamic modeling. *International Journal of Materials Research* **2006,** *97* (6), 845-853.
5. Kresse, G.; J. Furthmuller, Efficient iterative schemes for ab initio total-energy calculations using a plane-wave basis set. *Physical Review B* **1996,** *54* (16), 11169-11186.
6. Blochl, P. E., PROJECTOR AUGMENTED-WAVE METHOD. *Physical Review B* **1994,** *50* (24), 17953-17979.
7. Perdew, J. P.; K. Burke; M. Ernzerhof, Generalized gradient approximation made simple (vol 77, pg 3865, 1996). *Physical Review Letters* **1997,** *78* (7), 1396-1396.
8. Perdew, J. P.; K. Burke; M. Ernzerhof, Generalized gradient approximation made simple. *Physical Review Letters* **1996,** *77* (18), 3865-3868.
9. Zhang, Y. S.; E. Majzoub; V. Ozolins; C. Wolverton, Theoretical Prediction of Metastable Intermediates in the Decomposition of Mg(BH4)(2). *Journal of Physical Chemistry C* **2012,** *116* (19), 10522-10528.
10. Togo, Atsushi; Isao Tanaka, First principles phonon calculations in materials science. *Scripta Materialia* **2015,** *108*, 1-5.
11. Mauri, F.; S. G. Louie, Magnetic susceptibility of insulators from first principles. *Physical Review Letters* **1996,** *76* (22), 4246-4249.
12. Mauri, F.; B. G. Pfrommer; S. G. Louie, Ab initio theory of NMR chemical shifts in solids and liquids. *Physical Review Letters* **1996,** *77* (26), 5300-5303.
13. Pickard, C. J.; F. Mauri, All-electron magnetic response with pseudopotentials: NMR chemical shifts. *Physical Review B* **2001,** *63* (24), 245101(13).
14. Thonhauser, T.; D. Ceresoli; A. A. Mostofi; N. Marzari; R. Resta; D. Vanderbilt, A converse approach to the calculation of NMR shielding tensors. *Journal of Chemical Physics* **2009,** *131* (10), 101101.
15. Kresse, G.; D. Joubert, From ultrasoft pseudopotentials to the projector augmented-wave method. *Physical Review B* **1999,** *59* (3), 1758-1775.
16. Kresse, G.; J. Furthmuller, Efficiency of ab-initio total energy calculations for metals and semiconductors using a plane-wave basis set. *Computational Materials Science* **1996,** *6* (1), 15-50.
17. Gowda, C. M.; F. Vasconcelos; E. Schwartz; E. R. H. van Eck; M. Marsman; Jjlm Cornelissen; A. E. Rowan; G. A. de Wijs; A. P. M. Kentgens, Hydrogen bonding and chemical shift assignments in carbazole functionalized isocyanides from solid-state NMR and first-principles calculations. *Physical Chemistry Chemical Physics* **2011,** *13* (28), 13082-13095.

18. Yates, J. R.; C. J. Pickard; F. Mauri, Calculation of NMR chemical shifts for extended systems using ultrasoft pseudopotentials. *Physical Review B* **2007,** *76* (2), 024401(11).
19. Mason, J., Conventions for the reporting of nuclear magnetic shielding (or shift) tensors suggested by participants in the NATO ARW on NMR shielding constants at the University-of-Maryland, College-Park, July 1992. *Solid State Nuclear Magnetic Resonance* **1993,** *2* (5), 285-288.
20. Caputo, R.; A. Tekin, Ab-initio crystal structure prediction. A case study: $NaBH_4$. *Journal of Solid State Chemistry* **2011,** *184* (7), 1622-1630.
21. Guella, G.; B. Patton; A. Miotello, Kinetic features of the platinum catalyzed hydrolysis of sodium borohydride from B-11 NMR measurements. *Journal of Physical Chemistry C* **2007,** *111* (50), 18744-18750.
22. Kim, E.; R. Kumar; P. F. Weck; A. L. Cornelius; M. Nicol; S. C. Vogel; J. Z. Zhang; M. Hartl; A. C. Stowe; L. Daemen; Y. S. Zhao, Pressure-driven phase transitions in $NaBH_4$: Theory and experiments. *Journal of Physical Chemistry B* **2007,** *111* (50), 13873-13876.
23. Aprà, E.; E. J. Bylaska; W. A. de Jong; N. Govind; K. Kowalski; T. P. Straatsma; M. Valiev; H. J. J. van Dam; Y. Alexeev; J. Anchell; V. Anisimov; F. W. Aquino; R. Atta-Fynn; J. Autschbach; N. P. Bauman; J. C. Becca; D. E. Bernholdt; K. Bhaskaran-Nair; S. Bogatko; P. Borowski; J. Boschen; J. Brabec; A. Bruner; E. Cauët; Y. Chen; G. N. Chuev; C. J. Cramer; J. Daily; M. J. O. Deegan; T. H. DunningJr.; M. Dupuis; K. G. Dyall; G. I. Fann; S. A. Fischer; A. Fonari; H. Früchtl; L. Gagliardi; J. Garza; N. Gawande; S. Ghosh; K. Glaesemann; A. W. Götz; J. Hammond; V. Helms; E. D. Hermes; K. Hirao; S. Hirata; M. Jacquelin; L. Jensen; B. G. Johnson; H. Jónsson; R. A. Kendall; M. Klemm; R. Kobayashi; V. Konkov; S. Krishnamoorthy; M. Krishnan; Z. Lin; R. D. Lins; R. J. Littlefield; A. J. Logsdail; K. Lopata; W. Ma; A. V. Marenich; J. Martin del Campo; D. Mejia-Rodriguez; J. E. Moore; J. M. Mullin; T. Nakajima; D. R. Nascimento; J. A. Nichols; P. J. Nichols; J. Nieplocha; A. Otero-de-la-Roza; B. Palmer; A. Panyala; T. Pirojsirikul; B. Peng; R. Peverati; J. Pittner; L. Pollack; R. M. Richard; P. Sadayappan; G. C. Schatz; W. A. Shelton; D. W. Silverstein; D. M. A. Smith; T. A. Soares; D. Song; M. Swart; H. L. Taylor; G. S. Thomas; V. Tipparaju; D. G. Truhlar; K. Tsemekhman; T. Van Voorhis; Á. Vázquez-Mayagoitia; P. Verma; O. Villa; A. Vishnu; K. D. Vogiatzis; D. Wang; J. H. Weare; M. J. Williamson; T. L. Windus; K. Woliński; A. T. Wong; Q. Wu; C. Yang; Q. Yu; M. Zacharias; Z. Zhang; Y. Zhao; R. J. Harrison, NWChem: Past, present, and future. *The Journal of Chemical Physics* **2020,** *152* (18), 184102.
24. Becke, Axel D., Density-functional thermochemistry. III. The role of exact exchange. *The Journal of Chemical Physics* **1993,** *98* (7), 5648-5652.
25. Devlin, F. J.; J. W. Finley; P. J. Stephens; M. J. Frisch, Ab Initio Calculation of Vibrational Absorption and Circular Dichroism Spectra Using Density Functional Force Fields: A Comparison of Local, Nonlocal, and Hybrid Density Functionals. *The Journal of Physical Chemistry* **1995,** *99* (46), 16883-16902.
26. Petersson, G. A.; Mohammad A. Al-Laham, A complete basis set model chemistry. II. Open-shell systems and the total energies of the first-row atoms. *The Journal of Chemical Physics* **1991,** *94* (9), 6081-6090.